

Intrinsic thermodynamic properties of the pyrochlore superconductor RbOs_2O_6 extracted by condensation energy analysis

M. Brühwiler,* S.M. Kazakov, J. Karpinski, and B. Batlogg

Laboratory for Solid State Physics, ETH Zürich, 8093 Zürich, Switzerland.

(Dated: November 7, 2018)

Abstract

We develop a general procedure for the analysis of bulk thermodynamic data of a superconductor for samples containing a metallic non-superconducting second phase. The method is based on the condensation energy and it allows the extraction of the intrinsic properties of a superconductor even for non-ideal samples. Applying this procedure to the recently discovered geometrically frustrated β -pyrochlore superconductor RbOs_2O_6 ($T_c = 6.4$ K) yields a Sommerfeld coefficient as high as $79 \mu\text{J}/\text{g}/\text{K}^2$ ($44 \text{mJ}/\text{mol}_{\text{f.u.}}/\text{K}^2$). RbOs_2O_6 is inferred to be a strong type-II superconductor ($\kappa(T_c) = 23$) in the intermediate-coupling regime similar to niobium ($\lambda_{\text{ep}} \approx 1$). From the upper critical field $\mu_0 H_{c2} \approx 6$ T at 0 K, we estimate a Ginzburg-Landau coherence length $\xi \approx 74 \text{Å}$. The condensation energy is $860 \mu\text{J}/\text{g}$ ($483 \text{mJ}/\text{mol}_{\text{f.u.}}$) resulting in $1/(8\pi) \cdot (\gamma_1 T_c^2)/\Delta U_1 \approx 0.15$, a value well in the range of conventional phonon-mediated superconductors. The superconducting electronic specific heat indicates conventional s-wave pairing. The experimental Sommerfeld coefficient of $44 \text{mJ}/\text{mol}_{\text{f.u.}}/\text{K}^2$ is about 4 times larger than the one found in band structure calculations. Together with the electron-phonon coupling constant $\lambda_{\text{ep}} \approx 1$ this leaves an additional $\lambda_{\text{add}} \approx 2.4$ for enhancement due to other mechanisms.

PACS numbers: 74.25.Op, 74.25.Bt, 74.70.-b

*Electronic address: bruehwiler@solid.phys.ethz.ch

I. INTRODUCTION

Thermodynamic studies of single phase superconductor samples are most desirable, yet it often proves difficult to synthesize samples which are 100 % pure. Especially in the initial phase of the discovery of a new superconducting material, synthesis methods usually are not as advanced as to synthesize perfect samples. At this stage a significant amount of a precursor material or a by-product often remains as a second component in the end product. Therefore, much care must be taken when extracting properties of the superconductor to ensure that these are intrinsic.

For meaningful physical statements, intensive quantities need to be evaluated, i.e. the measured extensive physical quantities need to be given per amount of substance (a.o.s.), per volume, or per mass. However, since the ratio of the two components is not known, or the second component is considered to contribute marginally, the quantities are usually given per *total* a.o.s., volume, or mass. Values calculated in this way can be significantly off the true value and require a more careful analysis.

The key issue therefore is extracting the fraction of each component present. When dealing with a superconducting sample containing a second *metallic* component, such an analysis is possible and is described here. Integrating the heat capacity to obtain the condensation energy of the superconductor gives a measure for the amount of the superconducting component. When several samples of different superconducting volume fractions are measured, the condensation energy obtained varies accordingly. From the systematic variation it is possible to specify the properties of the ideal sample.

Specific heat measurements on RbOs_2O_6 have shown that in the superconducting state a noticeable density of states at the Fermi level remains as $T \rightarrow 0$ K (Fig. 1). The residual Sommerfeld coefficient γ_r and normal-state coefficient γ vary among the various synthesis runs in a way that is a typical signature of the above described situation. We have therefore developed the appropriate analysis method described below.

RbOs_2O_6 is one of only four pyrochlore superconductors known to date, of which three were discovered very recently and belong to the same family. These are the α -pyrochlore $\text{Cd}_2\text{Re}_2\text{O}_7$ [1, 2, 3] and the β -pyrochlores $A\text{Os}_2\text{O}_6$, where $A = \text{Cs, Rb, or K}$ [4, 5, 6]. The pyrochlores exhibit inherent geometrical frustration due to the metal ions forming a network of corner-sharing tetrahedra. Thus, metallic pyrochlores constitute ideal systems to study to

what degree itinerant electrons are affected by a lattice which is known to cause geometrical frustration for interactions of localized magnetic moments.

As reported previously [7], RbOs_2O_6 is a conventional s-wave superconductor with a critical temperature $T_c = 6.4\text{ K}$. This analysis was based on specific heat measurements and evidence for s-wave symmetry was also given by penetration depth measurements by Khasanov et al. (Ref. [8]). Further support for conventional s-wave-type superconductivity in RbOs_2O_6 comes from ^{87}Rb NMR measurements by Magishi et al. [9]. Here, we shed new light onto this subject by applying the developed analysis to our data on RbOs_2O_6 . In particular, we provide evidence for an additional electronic mass enhancement beyond the contribution from electron-phonon coupling.

This article is divided into two parts: First, the condensation energy analysis is described and appropriate formulas derived. In the second part we apply the analysis to RbOs_2O_6 to extract its intrinsic thermodynamic parameters. For illustration purposes, we frequently refer to the Figures pertaining to RbOs_2O_6 already in the general section. Finally, we elaborate on some further aspects of the condensation energy analysis in the Appendices.

II. CONDENSATION ENERGY ANALYSIS

The starting point for our analysis is the experimentally measured extensive heat capacity \tilde{C}_p of a sample [18]. We assume that two components contribute to this heat capacity: component *one* is the superconductor, while component *two* is a normal metal:

$$\tilde{C}_p = \tilde{C}_1 + \tilde{C}_2. \quad (1)$$

The fact that the first component becomes superconducting enables us to extract the contribution to the heat capacity from each component by analyzing the condensation energy. We therefore call this procedure condensation energy analysis (CEA).

Because the relative contribution of each component is not known a priori, and because a sample dependent extensive heat capacity is not meaningful, an experimenter assumes the contribution \tilde{C}_2 of component two to be small and uses the total mass m of the sample to convert the heat capacity into an intensive form $C_p = \tilde{C}_p/m$. In this case, the heat capacity C_p is given in energy per temperature per mass (typically in $\mu\text{J/g/K}$). Due to the presence of a second component, this heat capacity is obviously not the correct heat capacity of

component one.

Usually the total mass of a sample is measured and conversion into an intensive form is performed using this mass. Consequently, in our analysis we will also assume the total mass to be known experimentally. As will be shown below, this results in the properties of the sample to be linear in the superconducting mass fraction.

The CEA not only allows the extraction of the intrinsic properties of the superconducting phase, it also does so without requiring any further knowledge about the second normal metallic component. We use the presence of varying amounts of this second component to specify the properties of the ideal sample: The heat capacity C_p/T for the superconductor vanishes for $T \ll T_c$, while the measured residual heat capacity is due to the second, metallic phase only. To a certain extent, it is possible to extract intrinsic thermodynamic properties of the second component as well. If we can actually identify component two, e.g. from XRD structure analysis, this extraction is possible to the full extent, as we show in the present example.

A. Definitions

The following definitions will prove useful in making formulas more readable:

$$\mu := \frac{\rho_1}{\rho_2} \quad \epsilon := \frac{\gamma_2}{\gamma_1}. \quad (2)$$

Here, ρ_1 and ρ_2 are the mass densities of the two components in mass per volume and μ is their ratio. γ_1 and γ_2 are the Sommerfeld coefficients of the two components in energy per mass per temperature squared (typically in $\mu\text{J/g/K}^2$) and ϵ is their ratio.

We further assign η_V to the superconducting volume fraction and η_m to the superconducting mass fraction:

$$\eta_V := \frac{V_1}{V}, \quad \eta_m := \frac{m_1}{m}. \quad (3)$$

V_i and m_i are the volume and mass of component i , while V and m are the total volume and total mass respectively, i.e. $V_1 + V_2 = V$ and $m_1 + m_2 = m$.

B. Parameters extracted from the measurement

The parameters which are readily extracted from specific heat measurements and also published as such are the Sommerfeld coefficients of the two-component system γ and γ_r

in the normal state and the superconducting state respectively. We call the Sommerfeld coefficient in the superconducting state γ_r "residual", because it results from the second component only, since the first one becomes superconducting with a vanishing heat capacity for $T \rightarrow 0$. We calculate these as a function of the superconducting mass fraction η_m , which is proportional to the condensation energy $\Delta U = \eta_m \cdot \Delta U_1$. $\Delta U_1 = \Delta U|_{\eta_m=1}$ is the condensation energy of the superconducting component. ΔU for a given sample is readily obtained by integrating the measured specific heat to obtain the entropy difference

$$\Delta S(T) = \int_T^{T_c} \frac{\Delta C_p(T')}{T'} dT' \quad (4)$$

and then integrating again to obtain

$$\Delta U(T) = \int_T^{T_c} \Delta S(T') dT'. \quad (5)$$

Here, $\Delta C_p := C_{0T} - C_{12T}$ is the difference in heat capacity between the superconducting and normal state. In the present study, the normal state is reached by applying an external magnetic field of 12 T, which is well above the upper critical field. The thermodynamic critical field H_c is obtained from the condensation energy by using the relation $\frac{1}{2}\mu_0 H_c^2(T) = \Delta U_1(T)\rho_1 = \eta_m^{-1}\Delta U(T)\rho_1$.

The relations between the intrinsic Sommerfeld coefficients of the two components, γ_1 and γ_2 , and the measured Sommerfeld coefficients γ and γ_r are most easily obtained from their respective extensive forms:

The residual Sommerfeld coefficient $\tilde{\gamma}_r$ measured in 0 T is equivalent to the Sommerfeld coefficient $\tilde{\gamma}_2$ of the second component, since the density of states of the superconducting component is gapped and therefore $\gamma_1 = 0$:

$$m\gamma_r = \tilde{\gamma}_r = \tilde{\gamma}_2 = m_2\gamma_2. \quad (6)$$

From this we get

$$\gamma_r = -\gamma_2\eta_m + \gamma_2. \quad (7)$$

The residual Sommerfeld coefficient γ_r measured in 0 T is a direct measure for the presence of the second component. It is easily seen that the y -intercept of a γ_r vs η_m plot is equal to γ_2 and that γ_r vanishes at $\eta_m = 1$ and thus defines 100 % superconducting volume or mass fraction.

To calculate γ we equate

$$m\gamma = \tilde{\gamma} = \tilde{\gamma}_1 + \tilde{\gamma}_2 = m_1\gamma_1 + m_2\gamma_2, \quad (8)$$

resulting in

$$\gamma = (\gamma_1 - \gamma_2)\eta_m + \gamma_2, \quad (9)$$

which also depends linearly on the superconducting mass fraction η_m . Thus, from γ vs η_m , we get a second, independent plot to extract γ_2 by noting the y -intercept. Having located the ideal sample through γ_r , the intrinsic Sommerfeld coefficient of component one, γ_1 , can immediately be extracted by taking the value of γ at $\eta_m = 1$.

C. Superconducting electronic specific heat

The superconducting electronic specific heat C_{es} is extracted in the usual way by subtracting the specific heat at 0 T from the normal state specific heat at 12 T but paying attention to the appropriate masses:

$$\tilde{C}_{0\text{T}} = mC_{0\text{T}} = m_1C_{\text{es}} + \tilde{\gamma}_2T + \tilde{C}_{\text{lattice}} + \tilde{C}_{\text{other}} \quad (10)$$

$$\tilde{C}_{12\text{T}} = mC_{12\text{T}} = \tilde{\gamma}_1T + \tilde{\gamma}_2T + \tilde{C}_{\text{lattice}} + \tilde{C}_{\text{other}} + \tilde{C}_{\text{mag}}. \quad (11)$$

Here, C_{lattice} , C_{other} , and C_{mag} are the total heat capacity of both components from the respective source. C_{mag} describes any field-induced heat capacity, be it from fluctuations or from a magnetization of the material. Taking the difference and assuming any magnetic heat capacity C_{mag} to be negligible, we get

$$C_{\text{es}}(T) = \eta_m^{-1}\Delta C_{\text{p}} + \gamma_1T. \quad (12)$$

We conclude that the specific heat difference ΔC_{p} needs to be scaled with the inverse superconducting mass fraction to extract the true electronic superconducting specific heat. Also, the added electronic specific heat from the normal state, γ_1T , has to be calculated using the Sommerfeld coefficient γ_1 of the pure superconductor. For an ideal sample with $\eta_m = 1$, Eq. (12) is, of course, equivalent to the usual $C_{\text{es}}(T) = \Delta C_{\text{p}} + \gamma T$. As Figure 5 shows for RbOs_2O_6 , the electronic superconducting specific heat indeed shows a universal behavior when scaled appropriately according to Eq. (12).

At low temperatures, where $C_{\text{es}} \ll \gamma_1 T$, we can approximate ΔC_p using Eq. (12) and get

$$\Delta C_p = -\gamma_1 \eta_m T. \quad (13)$$

That is, ΔC_p is linear in T and the slope is proportional to η_m , varying from sample to sample. This behavior is illustrated in Fig. 2 for RbOs_2O_6 . Evidently, the negative of the mentioned slope plotted against the superconducting mass fraction has the value γ_1 at $\eta_m = 1$. ΔC_p thus provides another way of extracting the true Sommerfeld coefficient of component one from the data which is independent from γ vs η_m . It further provides an additional consistency check since this curve and γ vs η_m need to cross at the same η_m value as γ_r vs η_m vanishes (namely at $\eta_m = 1$).

If the assumptions on the composition of the samples leading to the CEA are correct, then the specific heat jump at T_c is proportional to the condensation energy:

$$\Delta C_p|_{T_c} = b \cdot \Delta U. \quad (14)$$

Here, b is a constant of proportionality thermodynamically related to the critical field by Eq. (15).

D. Discussion

As the analysis shows, the relevant parameter when measuring the total mass of a sample experimentally is the superconducting mass fraction η_m . All the relevant properties are linear in the mass fraction and therefore in the condensation energy, which can be readily extracted from specific heat measurements by integration. The reason for this is that the total mass m of the sample is used for the conversion from extensive into intensive form, not the volume or the a.o.s. In the case where another sample property is measured, the analysis remains analogous, but the parameters are linear in the corresponding superconducting fraction instead of the superconducting mass fraction. These variations are discussed in more detail in the Appendix.

We would like to mention, that though in principle still possible, performing the CEA would be more difficult when dealing with a nodal superconductor. In this case the superconducting heat capacity goes to zero not exponentially, but following a power-law. As a consequence, there is still some contribution from the superconductor to γ_r at all but the

very lowest temperatures. The same argument holds for the analysis of the slope of ΔC_p vs T (Eq. 13). The CEA would still work fine, but data to even lower temperatures might be needed.

Plotting the data as in Fig. 3 (here for RbOs_2O_6) allows γ_1 , γ_2 , and ΔU_1 to be extracted at a glance. At the same time, the plot serves as a check for the consistency of the analysis, since it is immediately apparent if the lines cross each other and the x - and y -axes at the correct points: γ_r needs to vanish at the same η_m value as γ vs η_m and the slope of $\Delta C_p(T)$ vs η_m cross. Also, the y -intercepts of γ vs η_m and γ_r vs η_m need to be the same.

We would like to comment on the necessity to pinpoint $\eta_m = 1$ for the extraction of the intrinsic parameters. In this study we accomplish this by extrapolating γ_r to zero which is possible because the second component is metallic and thus has a non-vanishing γ_2 . It is conceivable that $\eta_m = 1$ could also be pinpointed using some other technique. The ratio $\Delta C_p|_{T_c}/(\gamma_1 T_c)$ is a constant as a function of η_m if $\gamma_2 = 0$ and therefore it can be determined using a single sample with an arbitrary volume fraction as long as $\gamma_2 = 0$. b is always independent of η_m since it is the proportionality factor between $\Delta C_p|_{T_c}$ and ΔU . If the true condensation energy ΔU_1 is to be extracted, we need to locate $\eta_m = 1$ in any case. Since the normalized critical field slope Q (defined in Tab. I) and b are related thermodynamically, also Q can be determined independently of $\eta_m = 1$. In the case where $\gamma_2 = 0$, it follows that $\gamma = \eta_m \gamma_1$ and thus $\gamma_1/\Delta U_1 = \gamma/\Delta U$ rendering $1/(8\pi) \cdot (\gamma_1 T_c^2)/\Delta U_1$ independent of η_m . The Sommerfeld coefficient γ_1 is only independent of η_m if $\gamma_1 = \gamma_2$ (Eq. (9)). The reduced critical field h_c and the deviation function $D(t)$ (defined later in the text) are independent of η_m since $\Delta U_1(T)/\Delta U_1(0\text{ K}) = \Delta U(T)/\Delta U(0\text{ K})$. In summary, b , Q , h_c , and $D(t)$ can be determined using a single sample regardless of its superconducting mass fraction. $\Delta C_p|_{T_c}/(\gamma_1 T_c)$ and $1/(8\pi) \cdot (\gamma_1 T_c^2)/\Delta U_1$ can be extracted with a single sample if $\gamma_2 = 0$ but several samples are needed if $\gamma_2 \neq 0$. For $\Delta U_1(0\text{ K})$ and γ_1 it is imperative to measure many samples with different superconducting mass fractions and perform the CEA. There is only one improbable exception: If $\gamma_1 = \gamma_2$, γ_1 is independent of the superconducting mass fraction. These findings are listed in Tab. I.

Since the jump in the heat capacity $\Delta C_p|_{T_c}$ is proportional to ΔU , thermodynamic parameters may be analyzed in terms of $\Delta C_p|_{T_c}$ instead of $\Delta U = \Delta U_1 \eta_m$. This may eliminate some scatter in the data because $\Delta C_p|_{T_c}$ is more directly determined than ΔU . Since in this case the condensation energy ΔU_1 remains unknown, however, many intrinsic param-

TABLE I: Compilation of thermodynamic parameters for the extraction of which it is (a) necessary, (b) necessary if $\gamma_2 \neq 0$, and (c) not necessary to locate the ideal sample ($\eta_m = 1$). When dealing with a metallic second component, it is therefore essential to perform the condensation energy analysis for the cases (a) and (b).

Parameter	Classification
$\Delta U_1(0\text{ K})$	(a)
γ_1	(a), if $\gamma_1 \neq \gamma_2$
$\Delta C_p _{T_c}/(\gamma_1 T_c)$	(b)
$\frac{1}{8\pi} \frac{\gamma_1 T_c^2}{\Delta U_1}$	(b)
b	(c)
$Q \equiv -\frac{2T_c}{H_c(0)} \left. \frac{dH_c}{dT} \right _{T_c}$	(c)
$h_c(t), D(t)$	(c)

eters cannot be extracted. This alternative approach is particularly helpful when the heat capacity data do not extend to low enough temperature to yield the condensation energy by integration, nevertheless enabling the determination of the intrinsic γ_1 , γ_2 , and $\Delta C_p|_{T_c}$.

III. APPLICATION TO RbOs₂O₆

Using varied conditions in the preparation procedure, RbOs₂O₆ samples with superconducting volume fractions from 34 % to 83 % have been prepared. The varying superconducting fraction, which is an important prerequisite for the application of the CEA, is caused by the presence of OsO₂ as determined by X-ray diffraction analysis. We have therefore also measured a sample of the starting material OsO₂ and included it in the data analysis.

The polycrystalline samples all show the transition to the bulk superconducting state in resistivity and magnetization measurements. They typically weigh about 10 to 20 mg. The samples, labeled A to F, have been synthesized by a procedure originally described in Ref. [6] and described in more detail in Ref. [10]. An overview over the measured parameters is provided in Tab. II.

The specific heat was measured in a physical properties measurement apparatus using an adiabatic relaxation technique (Quantum Design, PPMS). Figure 1 shows the specific

TABLE II: Overview over the parameters extracted from the six samples measured in this study. The superconducting volume fractions η_V range from 34 % to 83 % due to varied conditions in the synthesis procedure.

	A	B	C	D	E	F
γ ($\mu\text{J}/\text{g}/\text{K}^2$)	35.5	54.3	60.7	61.7	58.8	65.0
β ($\mu\text{J}/\text{g}/\text{K}^4$)	3.26	1.38	2.23	0.72	1.22	1.60
γ_r ($\mu\text{J}/\text{g}/\text{K}^2$)	17.5	14.8	15.2	8.9	7.7	4.6
$-\frac{d(\Delta C_p)}{dT}$ ($\mu\text{J}/\text{g}/\text{K}^2$)	21.7	40.8	47.8	53.5	52.5	62.0
$\Delta U(0\text{ K})$ ($\mu\text{J}/\text{g}$)	211	378	465	528	607	644
T_c (K) ^a	6.25	6.22	6.36	6.36	6.47	6.37
Est. svf $\frac{\gamma-\gamma_r}{\gamma}$ (%) ^c	50.7	72.7	75.0	85.6	86.9	92.9
Svf η_V (%) ^{b c}	34.0	55.5	65.1	71.6	79.2	82.6
Rel. error (%) ^b	49.0	31.2	15.1	19.5	9.7	12.6
Smf η_m (%) ^c	24.5	44.0	54.1	61.4	70.6	74.9

^aFrom C_p/T vs T data (Fig. 1).

^bWith the second component being OsO_2 , $\mu \approx 0.63$.

^csvf: superconducting volume fraction, smf: superconducting mass fraction.

heat C_p/T vs T for two exemplary samples in the superconducting and normal state (0 T and 12 T). The residual Sommerfeld coefficient γ_r , the normal-state coefficient γ , and the specific heat jump at T_c , $\Delta C_p|_{T_c}/T_c$, vary among the various samples measured in a way that is a typical signature of a metallic second component. These observations form the basis for the condensation energy analysis (CEA) presented above. We therefore analyze our data on RbOs_2O_6 accordingly.

A. Normal state properties and determination of the condensation energy ΔU_1

From the normal-state curves at 12 T, we extract the Sommerfeld coefficients $\gamma = \lim_{T \rightarrow 0\text{ K}} C_p/T$ by fitting the data from 1 K to 4 K to $C_p/T = \gamma + \beta T^2 + DT^4$. The D -coefficients obtained by this fit procedure are essentially zero. Fits performed with restraining D to zero result in γ values differing by only 0.6 % or less compared to the ones where

D is not restrained. The only exception is sample A with a difference of 2.8 %, which we attribute to an impurity concentration. We have used data down to 1 K only for the fits because moderate contributions to the heat capacity can be expected from the nucleus of Rb at the lowest temperatures [19]. The upper temperature limit of 4 K is chosen such as to avoid any influence of possible low-lying non-Debye like modes, which cannot be parameterized by $C_p/T = \gamma + \beta T^2$.

The residual coefficient γ_r is the C_p/T value at 1 K and 0 T and T_c is chosen such as to balance the entropy (refer to Fig. 1). We further extract the negative of the slope of ΔC_p vs T , which at low temperatures is proportional to η_m (Eq. (13), Fig. 2). The values obtained for the various samples are summarized in Tab. II.

The actual integration for the entropy difference ΔS according to Eq. (4) is performed from 0 K to T using the relation $\int_T^{T_c} = \int_{0K}^{T_c} - \int_{0K}^T$ and assuming balanced entropy, i.e. $\int_{0K}^{T_c} \Delta C_p/T' dT' = 0$. To integrate starting from 0 K, the C_p/T curves have to be extrapolated to 0 K from their lowest value at 0.5 K. For this purpose we use the fitted Sommerfeld coefficients γ (s. Tab. II) for the C_p/T value at 0 K for the 12 T curves. Similarly, we use the C_p/T value at the lowest temperature of the 0 T curve and use it to extrapolate a constant C_p/T to 0 K. The resulting ΔS curves are shown in the inset of Fig. 2 and the condensation energies $\Delta U(0\text{ K})$ are listed in Tab. II. The $\Delta U(T)$ curves derived by integrating $\Delta S(T)$ (Eq. (5)) were also obtained using the relation $\int_T^{T_c} = \int_{0K}^{T_c} - \int_{0K}^T$ together with $\int_{0K}^{T_c} \Delta S dT' = \Delta U(0\text{ K})$.

The essential steps of the CEA are shown in Fig. 3: The measured Sommerfeld coefficient γ , the residual Sommerfeld coefficient γ_r , and the slope from ΔC_p vs T at low temperatures are plotted as a function of the condensation energy ΔU . All these quantities are directly extracted from measurement and they all depend linearly on the superconducting mass fraction $\eta_m = \Delta U/\Delta U_1$, see Eqs. (7), (9), and (13). We therefore perform a linear fit of these data calling the fitted lines γ -line, γ_r -line, and ΔC_p -slope-line respectively, and use them to extract parameters and perform consistency checks. For the fit of the γ -line only we have included the data point resulting from the OsO₂ sample ($\gamma_2 = 27.5 \mu\text{J/g/K}^2$ at $\Delta U = 0$).

For the fit of the ΔC_p -slope-line we have refrained from restraining the y -intercept to 0, even though it would be justified from Eq. (13). This results in a small, finite intercept which we attribute to a minute C_{mag} rather than systematic error in ΔU , since ΔC_p vs ΔU

shows no similar offset. This explanation is also suggested by the heat capacity data at 12 T and 0 T, which slightly differ above T_c . This minute refinement will be further discussed later in the context of C_{es} and in Appendix D.

The fully superconducting sample, i.e. the sample with $\eta_m = \eta_V = 1$, is defined by the x -intercept of the γ_r -line. This defines the value of $\Delta U|_{\eta_m=1}$ and with that it defines the condensation energy ΔU_1 of the superconductor. The value obtained in this way for ΔU_1 is $872 \mu\text{J/g}$. The y -intercept of the γ_r -line of $(25.3 \pm 3) \mu\text{J/g/K}^2$ agrees well with the measured Sommerfeld coefficient γ_2 of OsO_2 of $27.5 \mu\text{J/g/K}^2$, providing a self-consistency check.

The Sommerfeld coefficient of component one, γ_1 , is the ordinate at the point where the γ -line and the ΔC_p -slope-line cross. According to the CEA, this happens at $\eta_m = 1$, i.e. at the same η_m value as γ_r vanishes. The crossing point thus is another means to find $\eta_m = 1$. The point of intersection of the two lines is at $849 \mu\text{J/g}$, in good agreement with the $872 \mu\text{J/g}$ obtained from the γ_r -line. As the effective ΔU_1 value we thus use $860 \mu\text{J/g}$ ($483 \text{ mJ/mol}_{f.u.}$), yielding a Sommerfeld coefficient for RbOs_2O_6 of $\gamma_1 = 79 \mu\text{J/g/K}^2$ ($44 \text{ mJ/mol}_{f.u./K}^2$).

In this study, we have performed separate linear fits for the γ -line, γ_r -line, and ΔC_p -slope-line respectively. Good agreement among the γ_2 and ΔU_1 values obtained with independent lines confirm that our assumptions on the composition of the samples (motivated by the X-ray diffractograms) leading to the CEA are correct. For further refinement of the parameters, it would thus be appropriate to perform a simultaneous fit of all three lines with constraints on the relevant intercepts.

B. Superconducting properties and density of states enhancement

The specific heat jump at T_c , $\Delta C_p|_{T_c}/T_c$, is extracted from the C_p/T vs T plot in Fig. 1 and plotted vs ΔU in Fig. 4. As expected, $\Delta C_p|_{T_c}/T_c$ is proportional to the condensation energy ΔU . A linear fit using $\Delta C_p|_{T_c}/T_c = b/T_c \cdot \Delta U$ with b/T_c as a fit parameter gives $b/T_c = (0.175 \pm 0.005) \text{ K}^{-2}$, and a specific heat jump for the pure superconductor of $\Delta C_p|_{T_c}/T_c = 150.5 \mu\text{J/g/K}^2$. This results in a normalized specific heat anomaly $\Delta C_p|_{T_c}/(\gamma_1 T_c) = 1.9$. The accuracy of this value depends mainly on the accuracy of the condensation energy ΔU_1 , since the error in b/T_c is rather small. Since both γ and $\Delta C_p|_{T_c}/T_c$ are linear in ΔU with a positive slope (in the case of RbOs_2O_6), the ratio $\Delta C_p|_{T_c}/(\gamma_1 T_c)$ is relatively stable against an error in ΔU .

TABLE III: Thermodynamic parameters of RbOs₂O₆.

Parameter	Value
$\xi(0\text{ K})$	74 Å
$\lambda_{\text{eff}}(0\text{ K})$	252 nm
$\kappa(T_c), \kappa(0\text{ K})$	23, 34
$\Delta C_p _{T_c}/(\gamma_1 T_c)$	1.9
λ_{ep}	1 ± 0.1
b	$(1.12 \pm 0.03)\text{ K}^{-1}$ ^a
b/T_c	$(0.175 \pm 0.005)\text{ K}^{-2}$ ^a
$\Delta U_1(0\text{ K})$	860 μJ/g (483 mJ/mol _{f.u.})
$H_c(0\text{ K})$	1249 Oe
$H_{c1}(0\text{ K})$	92 Oe
$H_{c2}(0\text{ K})$	60000 Oe ^b
$-dH_c/dT _{T_c}$	369 Oe/K
$-dH_{c2}/dT _{T_c}$	12000 Oe/K ^b
$Q \equiv -\frac{2T_c}{H_c(0)} \frac{dH_c}{dT} _{T_c}$	3.79 ± 0.05
$k_B T_c/(\hbar\omega_{\text{ln}})$	0.06
$\frac{2\Delta(0\text{ K})}{k_B T_c}$	3.87
$\frac{1}{8\pi} \frac{\gamma_1 T_c^2}{\Delta U_1}$	0.15
γ_1	$79 \mu\text{J/g/K}^2$ (44 mJ/mol _{f.u.} /K ²)

^a $b \cdot T_c = Q^2/2$ has a universal value of 5.99 for a weak coupling BCS superconductor. This results in $b/T_c = 0.146\text{ K}^{-2}$ and $b = 0.94\text{ K}^{-1}$ for a BCS superconductor with $T_c = 6.4\text{ K}$.

^bFrom Ref. [7]

The normalized specific heat jump $\Delta C_p|_{T_c}/(\gamma_1 T_c) = 1.9$ is significantly larger than that for the weak-coupling case (1.43). It corresponds to an electron-phonon coupling constant $\lambda_{\text{ep}} = 2 \int_0^\infty \alpha^2 F(\omega)/\omega d\omega \approx 1$ [11], i.e. RbOs₂O₆ is a superconductor in the intermediate-coupling regime. Here, $\alpha^2 F(\omega)$ is the electron-phonon spectral density. Using the calculated band Sommerfeld coefficient $\gamma_b = 17.8\text{ μJ/g/K}^2$ of RbOs₂O₆ from Ref. [12], the present result indicates a significant enhancement of the electronic specific heat of

$(1 + \lambda_{\text{ep}} + \lambda_{\text{add}}) = (79.1 \mu\text{J/g/K}^2)/(17.8 \mu\text{J/g/K}^2) \approx 4.4$. This enhancement surpasses the one found in Sr_2RuO_4 of about 3.8 by 16% [13]. Additional to the electron-phonon enhancement λ_{ep} , there is a strong enhancement of unknown origin $\lambda_{\text{add}} \approx 2.4$. We use the band structure γ_{b} from another Reference to estimate the uncertainty in this additional enhancement: Saniz et al. (Ref. [13]) have calculated the band Sommerfeld coefficient for KOs_2O_6 , which is 18% higher than the one calculated in Ref. [12]. Assuming these 18% to be the uncertainty in γ_{b} for RbOs_2O_6 , this would result in a $\lambda_{\text{add}} \approx 2.1 \pm 0.3$. In view of a calculated Stoner enhancement of the magnetic susceptibility of roughly 2 [12], we speculate that the additional enhancement is due to spin correlation effects.

From $\Delta U_1(0\text{ K})$ we calculate a thermodynamic critical field $H_c(0\text{ K}) = 1249\text{ Oe}$. Together with the exact thermodynamic relationship

$$\left. \frac{dH_c}{dT} \right|_{T_c} = \frac{-1}{\sqrt{2}} \sqrt{b/T_c} H_c(0\text{ K}) \quad (15)$$

this gives a critical field slope of $-dH_c/dT|_{T_c} = 369\text{ Oe/K}$. The same relationship gives the normalized critical field slope (also called "Q" in literature) $Q \equiv -\frac{2T_c}{H_c(0)} \left. \frac{dH_c}{dT} \right|_{T_c} = \sqrt{2bT_c} = 3.79 \pm 0.05$. To calculate the Ginzburg-Landau parameter κ at T_c , we use

$$\kappa(T_c) = \frac{1}{\sqrt{2}} \frac{\left. \frac{dH_{c2}}{dT} \right|_{T_c}}{\left. \frac{dH_c}{dT} \right|_{T_c}} = \frac{-\left. \frac{dH_{c2}}{dT} \right|_{T_c}}{\sqrt{b/T_c} H_c(0\text{ K})} \quad (16)$$

to get $\kappa(T_c) = 23$. For this we have used $-dH_{c2}/dT|_{T_c} = 12000\text{ Oe/K}$ from Ref. [7]. At 0 K we use $\kappa(0\text{ K}) = 1/\sqrt{2} \cdot H_{c2}(0\text{ K})/H_c(0\text{ K})$ to get $\kappa(0\text{ K}) = 34$ using a reasonably extrapolated $H_{c2}(0\text{ K}) = 60000\text{ Oe}$ [7]. Using

$$\lambda_{\text{eff}} = \sqrt{\frac{\kappa \Phi_0}{2\sqrt{2}\pi\mu_0 H_c}}, \quad (17)$$

where Φ_0 is the magnetic flux quantum, we get the penetration depth $\lambda_{\text{eff}}(0\text{ K}) = 252\text{ nm}$. This is fairly close to the estimated 230 nm obtained from magnetization measurements in Ref. [8] and somewhat larger than the 212 nm obtained from an analysis in Ref. [14]. The Ginzburg-Landau coherence length results in $\xi(0\text{ K}) = \lambda_{\text{eff}}(0\text{ K})/\kappa(0\text{ K}) \approx 74\text{ \AA}$. Finally, the lower critical field results from

$$H_{c1} = \frac{\ln \kappa}{\sqrt{2}\kappa} H_c \quad (18)$$

and gives $H_{c1}(0\text{ K}) = 92\text{ Oe}$.

Using the approximate semiphenomenological forms of the strong-coupling correction to the weak coupling BCS ratios which hold for many superconductors [15],

$$\frac{\Delta C_p|_{T_c}}{\gamma_1 T_c} = 1.43 \left[1 + 53 \left(\frac{k_B T_c}{\hbar \omega_{\text{ln}}} \right)^2 \ln \left(\frac{\hbar \omega_{\text{ln}}}{3 k_B T_c} \right) \right] \quad (19)$$

and

$$\frac{2\Delta(0\text{ K})}{k_B T_c} = 3.53 \left[1 + 12.5 \left(\frac{k_B T_c}{\hbar \omega_{\text{ln}}} \right)^2 \ln \left(\frac{\hbar \omega_{\text{ln}}}{2 k_B T_c} \right) \right], \quad (20)$$

we get a strong-coupling parameter $k_B T_c / (\hbar \omega_{\text{ln}}) = 0.06$ and $2\Delta(0\text{ K}) / (k_B T_c) = 3.87$. Here $\hbar \omega_{\text{ln}}$ is the Allen-Dynes expression for the average phonon energy. The Sommerfeld coefficient, the condensation energy, and the critical temperature result in $1/(8\pi) \cdot (\gamma_1 T_c^2) / \Delta U_1 = 0.15$, a value well in the range of conventional phonon-mediated superconductors [15].

The values discussed in the previous sections are summarized in Tab. III.

We extract the superconducting electronic specific heat $C_{\text{es}}(T)$ in the way described according to Eq. (12). To correct for the metallic second component present, the specific heat difference ΔC_p needs to be scaled with the inverse superconducting mass fraction and the added electronic specific heat from the normal state, $C_{\text{en}}(T) = \gamma_1 T$, has to be calculated using the Sommerfeld coefficient γ_1 of the pure superconductor. As Figure 5 shows, the electronic superconducting specific heat for various samples indeed shows a universal behavior when scaled appropriately.

The data at very low temperatures are susceptible to even a minute C_{mag} term present in the 12 T heat capacity (c.f. Eq. (10)). For a logarithmic plot of C_{es} , where the behavior at low temperatures is much expanded, it is therefore necessary to further fine-tune the CEA and account for such a small additional term. A contribution consistent with the deviation of the y -intercept from 0 of the ΔC_p -slope-line (Fig. 3) amounts to a few percent of the normal state specific heat $\gamma_1 T$. The refined analysis results in a superconducting electronic specific heat for RbOs_2O_6 shown in the inset of Fig. 5 on a logarithmic scale. The details of this refined analysis are elaborated later in Appendix D. It decreases in close quantitative agreement with conventional superconducting behavior. The solid line is a best fit to the data and indicates the expected behavior from an isotropic gap: $C_{\text{es}} = 9 \gamma_1 T_c \exp(-1.55 T_c/T)$. The dash-dotted line from weak coupling BCS also assuming an isotropic gap is shown for comparison: For $2.5 < T_c/T < 6$, the specific heat approximately follows an exponential behavior $C_{\text{es}} = 8.5 \gamma T_c \exp(-1.44 T_c/T)$ [16]. At low temperatures, the subtraction provides

unreliable results, since the difference becomes exceedingly small. Furthermore, scattering from various minute impurities may play a role at such low temperatures, and it is thus difficult to draw conclusions from the observed deviation.

We calculate the reduced critical field $h_c(t) := H_c(T)/H_c(0\text{ K}) = \sqrt{\Delta U_1(T)/\Delta U_1(0\text{ K})}$ which is independent of the superconducting mass fraction of a sample, because η_m cancels when taking the ratio $\Delta U_1(T)/\Delta U_1(0\text{ K})$ (Tab. I). The deviation function $D(t) := h_c(t) - (1 - t^2)$, where $t := T/T_c$, measures the deviation of the critical field from a simple $1 - t^2$ behavior. Figure 6 shows both these quantities as a function of temperature for sample F. The deviation function of RbOs_2O_6 closely matches that of Nb from Ref. [17], which is in line with the observation that the coupling constant $\lambda_{\text{ep}} \approx 1$ is the same as that of Nb, within experimental uncertainty.

IV. CONCLUSION

A detailed analysis is presented for the extraction of bulk thermodynamic parameters for samples containing a superconductor of interest and a second metallic non-superconducting component. Since parameter *estimates* can be significantly off even for large superconducting fractions, the analysis is essential for the extraction of intrinsic properties. We have developed all the formulas necessary for the analysis and point to important consistency checks. We apply the analysis, which we call condensation energy analysis (CEA), to RbOs_2O_6 to extract its intrinsic thermodynamic parameters. The main results are as follows: RbOs_2O_6 is a strong type-II superconductor ($\kappa(T_c) = 23$) in the intermediate-coupling regime comparable to niobium ($\lambda_{\text{ep}} \approx 1$). From the upper critical field $\mu_0 H_{c2} \approx 6\text{ T}$ at 0 K, we estimate a Ginzburg-Landau coherence length $\xi \approx 74\text{ \AA}$. The condensation energy is $860\text{ }\mu\text{J/g}$ ($483\text{ mJ/mol}_{\text{f.u.}}$) resulting in $1/(8\pi) \cdot (\gamma_1 T_c^2)/\Delta U_1 \approx 0.15$, a value well in the range of conventional phonon-mediated superconductors. The superconducting electronic specific heat indicates conventional s-wave pairing. RbOs_2O_6 has a high Sommerfeld coefficient for a pyrochlore of $79\text{ }\mu\text{J/g/K}^2$ ($44\text{ mJ/mol}_{\text{f.u.}}/\text{K}^2$) and thus a remarkably large enhancement over the calculated band coefficient of 3.8 to 4.4. We speculate that the origin of this mass enhancement lies in the 3-dimensional triangular nature of the pyrochlore lattice.

This study was partly supported by the Swiss National Science Foundation.

- [1] M. Hanawa, Y. Muraoka, T. Tayama, T. Sakakibara, J. Yamaura, and Z. Hiroi, *Phys. Rev. Lett.* **87**, 187001 (2001).
- [2] H. Sakai, K. Yoshimura, H. Ohno, H. Kato, S. Kambe, R. E. Walstedt, T. D. Matsuda, Y. Haga, and Y. Onuki, *J. Phys.: Condens. Matter* **13**, L785 (2001).
- [3] R. Jin, J. He, S. McCall, C. S. Alexander, F. Drymiotis, and D. Mandrus, *Phys. Rev. B* **64**, 180503 (2001).
- [4] S. Yonezawa, Y. Muraoka, and Z. Hiroi, *J. Phys. Soc. Jpn.* **73**, 1655 (2004).
- [5] S. Yonezawa, Y. Muraoka, Y. Matsushita, and Z. Hiroi, *J. Phys. Soc. Jpn.* **73**, 819 (2004).
- [6] S. Yonezawa, Y. Muraoka, Y. Matsushita, and Z. Hiroi, *J. Phys.: Condens. Matter* **16**, L9 (2004).
- [7] M. Brühwiler, S. M. Kazakov, N. D. Zhigadlo, J. Karpinski, and B. Batlogg, *Phys. Rev. B* **70**, 020503(R) (2004).
- [8] R. Khasanov, D. G. Eshchenko, J. Karpinski, S. M. Kazakov, N. D. Zhigadlo, R. Brütsch, D. Gavillet, D. Di Castro, A. Shengelaya, F. La Mattina, et al., *Phys. Rev. Lett.* **93**, 157004 (2004).
- [9] K. Magishi, J. L. Gavilano, B. Pedrini, J. Hinderer, M. Weller, H. R. Ott, S. M. Kazakov, and J. Karpinski, *cond-mat/0409169*.
- [10] S. M. Kazakov, N. D. Zhigadlo, M. Brühwiler, B. Batlogg, and J. Karpinski, *Supercond. Sci. Technol.* **17**, 1169 (2004).
- [11] F. Marsiglio, J. M. Coombes, and J. P. Carbotte, *Phys. Rev. B* **35**, 3219 (1987).
- [12] J. Kunes, T. Jeong, and W. E. Pickett, *Physical Review B (Condensed Matter and Materials Physics)* **70**, 174510 (pages 6) (2004), URL <http://link.aps.org/abstract/PRB/v70/e174510>.
- [13] R. Saniz, J. E. Medvedeva, L.-H. Ye, T. Shishidou, and A. J. Freeman, *Phys. Rev. B* **70**, 100505(R) (2004).
- [14] T. Schneider, R. Khasanov, and H. Keller, *cond-mat/0409398*.
- [15] F. Marsiglio and J. P. Carbotte, *Phys. Rev. B* **33**, 6141 (1986).
- [16] J. Bardeen and J. R. Schrieffer, *Recent Developments in Superconductivity*, vol. III of *Progress*

in low temperature physics (north-holland, 1961).

[17] H. A. Leupold and H. A. Boorse, Phys. Rev. **134**, A1322 (1964).

[18] We use a tilde ($\widetilde{}$) to denote quantities in an extensive form. Often, a capital C is used to denote (extensive) heat capacity, while a small c is used to denote (intensive) specific heat, i.e. $c = C/m$. For several reasons, this notation is not appropriate here. First, we also use heat capacity per volume and a.o.s., for which there is no dedicated symbol. Second, the same difficulty of an extensive/intensive quantity applies to the Sommerfeld coefficient γ , for which there is only one customary symbol. We therefore feel that a tilde is a more advisable way to distinguish extensive from intensive quantities. Further, the terms "specific heat" and "heat capacity" are often used interchangeably and we therefore prefer to use the terms intensive/extensive heat capacity instead.

[19] We write the contribution from the Rb nucleus in the usual high temperature expanded form $C_{\text{nuc}} = \eta_m A (\mu_0 H / T)^2$, where η_m accounts for the non-ideal samples and $A = 3.54 \text{ nJ/g} \cdot \text{K/T}^2$. At $\mu_0 H = 12 \text{ T}$ the nuclear heat capacity amounts to a negligible $C_{\text{nuc}} / (\gamma_1 T) \approx 0.6\%$ at 1 K and a moderate 7% at 0.45 K.

APPENDIX A: APPROXIMATIONS

To perform the CEA, more than one sample needs to be measured with the samples having various fractions of component one and two. If only the data from one sample is available, it is possible to approximate the Sommerfeld coefficient and the superconducting volume fraction to some extent. The validity of the approximations depends on the properties of the material under investigation.

1. Sommerfeld coefficient

The true Sommerfeld coefficient of component one, γ_1 , may be approximated by dividing the Sommerfeld coefficient γ by the estimated superconducting volume fraction $(\gamma - \gamma_r)/\gamma$ (see below):

$$\frac{\gamma^2}{\gamma - \gamma_r} = \gamma_1 + \delta(2\gamma_2 - \gamma_1) + \delta^2 \frac{\gamma_2^2}{(1 - \delta)\gamma_1} \xrightarrow{\delta \rightarrow 0} \gamma_1, \quad (\text{A1})$$

where $\delta := 1 - \eta_m$ is the deviation from the ideal sample. This approximation is easily calculated from the measured coefficients γ and γ_r and also makes sense intuitively. A criterion ensuring that $\gamma^2/(\gamma - \gamma_r)$ is a better approximation to γ_1 than γ itself is

$$\left| \frac{d}{d\eta_m} \Big|_{\eta_m=1} \left(\frac{\gamma^2}{\gamma - \gamma_r} \right) \right| = |\gamma_1 - 2\gamma_2| < |\gamma_1 - \gamma_2| = \left| \frac{d\gamma}{d\eta_m} \Big|_{\eta_m=1} \right|. \quad (\text{A2})$$

This criterion tests the rate of departure of the approximation $\gamma^2/(\gamma - \gamma_r)$ and the measured Sommerfeld coefficient γ from the true Sommerfeld coefficient γ_1 at $\eta_m = 1$. Strictly speaking, the criterion is thus only valid locally around $\eta_m = 1$. Depending on the material details, $\gamma^2/(\gamma - \gamma_r)$ or γ may be the better approximation at smaller volume fractions or they may both be useless altogether. At very small volume fractions, $\gamma^2/(\gamma - \gamma_r)$ is always a bad approximation, since it diverges like $1/\eta_m$.

How does the estimated Sommerfeld coefficient $\gamma^2/(\gamma - \gamma_r)$ compare to the measured coefficient γ in the case of RbOs_2O_6 ? Using the above determined values for γ_2 and γ_1 we find that the criterion Eq. (A2) is fulfilled: $|\gamma_1 - 2\gamma_2| = 24.1 \mu\text{J/g/K}^2 < 51.6 \mu\text{J/g/K}^2 = |\gamma_1 - \gamma_2|$. At high superconducting mass fractions, $\gamma^2/(\gamma - \gamma_r)$ is therefore a better approximation to γ_1 than γ . Fig. 7 shows that the estimate is reasonable down to about 20% superconducting mass fraction in RbOs_2O_6 .

2. Superconducting volume fraction

The true superconducting volume fraction is related to the superconducting mass fraction by

$$\eta_V = \frac{m_1/\rho_1}{m_1/\rho_1 + m_2/\rho_2} = \frac{\eta_m}{(1 - \mu)\eta_m + \mu}. \quad (\text{A3})$$

A possible approximation to η_V easily obtained from Eqs. (7) and (9) is the ratio $(\gamma - \gamma_r)/\gamma$ which is often used as an estimate:

$$\frac{\gamma - \gamma_r}{\gamma} = \frac{\eta_m}{(1 - \epsilon)\eta_m + \epsilon}. \quad (\text{A4})$$

This ratio is easily extracted from specific heat measurements and is therefore a popular way to extract the superconducting volume fraction. It has the same functional dependence on η_m as the true superconducting volume fraction, but it uses the parameter ϵ instead of μ . Depending on the materials under investigation, this estimate can therefore be significantly off: Comparing the estimate to the true superconducting volume fraction η_V , we get

$$\frac{\frac{\gamma - \gamma_r}{\gamma} - \eta_V}{\eta_V} = \frac{(\epsilon - \mu)(\eta_m - 1)}{\eta_m - \epsilon(\eta_m - 1)}. \quad (\text{A5})$$

The relative error therefore is at maximum when $\eta_m = 0$ and amounts to $(\mu - \epsilon)/\epsilon$. It can be very large depending on the mass densities, and the Sommerfeld coefficients of the components. Even at a large superconducting fraction, the error can be quite significant.

How does the estimated superconducting volume fraction $(\gamma - \gamma_r)/\gamma$ compare to the true superconducting volume fraction η_V in the case of RbOs_2O_6 ? In Fig. 8 we plot the true superconducting volume fraction and the estimated fraction as a function of the condensation energy ΔU . With OsO_2 as the second component, we calculated the parameter $\mu = \rho_1/\rho_2 \approx (7.215 \text{ g/cm}^3)/(11.445 \text{ g/cm}^3) \approx 0.63$ and use it to evaluate η_V . For the estimated fraction we have used the above values for γ_2 and γ_1 yielding $\epsilon \approx 0.35$. The Figure also shows the relative error (Eq. (A5)), which reaches a maximum of 80 % at $\eta_m = 0$.

APPENDIX B: GENERAL SEPARATION OF THE TWO COMPONENTS

In the main text we have extracted a few parameters of the heat capacity and analyzed them in terms of the superconducting mass fraction. This has allowed us to determine the parameters for an ideal sample at $\eta_m = 1$. We now want to extract the full temperature

dependence of the heat capacity of the two components $C_1(T)$ and $C_2(T)$ from the measured data.

To do this, we rewrite Eq. (1):

$$C_p(T) = \eta_m C_1(T) + (1 - \eta_m) C_2(T) \quad (\text{B1})$$

and we expand the heat capacities into power series:

$$C_p(T) = \sum_k a_k T^k \quad C_i(T) = \sum_k a_{i,k} T^k, \quad i \in \{1, 2\}. \quad (\text{B2})$$

From inserting the expansion (B2) into Eq. (B1) follows that

$$a_k = (a_{1,k} - a_{2,k})\eta_m + a_{2,k} \quad \forall k, \quad (\text{B3})$$

i.e. all coefficients a_k of the series expansion are linear in η_m .

Therefore, a general recipe to separate the measured quantity into its components is to expand it into a power series. The coefficients of the power series depend linearly on the superconducting mass fraction η_m and thus the intrinsic coefficients for component one ($a_{1,k}$) and two ($a_{2,k}$) can be extracted by a linear fit when a_k is plotted vs η_m . Using these coefficients, we can easily reconstruct $C_1(T)$ and $C_2(T)$.

Of course, the measured Sommerfeld coefficient γ together with the intrinsic coefficients γ_1 and γ_2 which were used in the main text are just a special case of the above analysis with $a_1 \equiv \gamma$, $a_{1,1} \equiv \gamma_1$, and $a_{2,1} \equiv \gamma_2$.

APPENDIX C: ALTERNATIVE SAMPLE PROPERTY MEASURED

As discussed in the main text, this analysis is necessary because the thermodynamic quantity of interest is an *intensive* heat capacity. However, since the relative fraction of the two phases is not known a priori, the mass (volume, a.o.s.) used to convert the extensive heat capacity into intensive heat capacity is the *total* mass (volume, a.o.s.) of the sample measured. This leads to an error in the heat capacity, which can be eliminated using the condensation energy analysis given above.

The set of formulas for the condensation energy analysis depends on the units the heat capacity is given in and the sample property measured (mass, volume, or a.o.s.). Whereas mass is the most often encountered case of a sample property measured, we also list the

formulas for other situations in Table IV. In the main text we have chosen to give the heat capacity per mass because this simplifies the equations when the total mass is measured. Considering our analysis, we propose that for practical purposes heat capacity should always be specified per sample property measured, i.e. per mass in the most cases. A mathematical conversion assuming a tabulated molar mass, for example, renders data inscrutable. Such conversions should only be done for parameters of an ideal sample.

APPENDIX D: INCLUSION OF A C_{mag} TERM

In Section III A of the main text we have attributed the deviation of the ΔC_p -slope-line y -intercept from zero to a finite magnetic heat capacity. Even though the deviation of the y -intercept is fairly small and may be attributed to measurement uncertainty, we nevertheless make an attempt to explain it here. It is shown that a refined analysis including a linear-in- T C_{mag} term can account for this behavior. In Section III B we have mentioned that a fine-tuned CEA including such a term is used for the extraction of $C_{\text{es}}(T)$ on a logarithmic scale, where the behavior at low temperatures is much expanded. The details of this refinement are given here as well. Further, it is shown that the inclusion of such a term leaves the extracted parameters practically unchanged.

To account for the magnetic heat capacity from various possible sources like magnetic impurities, magnons, or fluctuations, we may assume an approximate form $C_2^{\text{mag}} = \gamma_2^{\text{mag}}T$ to first order. This is reasonable considering that e.g. a Schottky-type impurity has a maximum C_p/T contribution around 2 to 5 K at 12 T, depending on the g -factor and the interaction strength. In this temperature region the extraction of both the Sommerfeld coefficient γ and the slope of ΔC_p are performed. Thus, traces of impurities may result in an additional "linear term" causing γ and $-d(\Delta C_p)/dT$ to increase.

Traces of magnetic impurities have been identified in the starting material and additional impurity phases like RbOsO_4 may be produced by the synthesis procedure. We would like to emphasize that such phases are present in the ppm range in vast contrast to the 17 to 66 volume-percent OsO_2 , the component relevant for the CEA. Magnetic trace impurities are merely mentioned here to motivate the inclusion of the additional small term γ_2^{mag} . As will be shown below, the extracted parameters are essentially unchanged and thus the inclusion of $\gamma_2^{\text{mag}}T$ is a "second order" extension to the analysis.

TABLE IV: Formula sets for the CEA describing parameters as a function of the superconducting fraction. Cases where the heat capacity is given per sample property measured are given in the first three sets, from which the first set is used in this article. $\eta_m = n_1/n$ denotes the superconducting a.o.s. fraction. The last set (measured mass, heat capacity per a.o.s.) is the most frequently encountered situation in publications and is therefore listed here as well. In this case the formulas include the factor $\nu = M_1/M_2$ which is the ratio of the molar masses of the two components. We use the expansion $C_p(T) = \sum_k a_k T^k$ and $C_i(T) = \sum_k a_{i,k} T^k$, where $i \in \{1, 2\}$, for the heat capacity, so e.g. $a_1 \equiv \gamma$, $a_{1,1} \equiv \gamma_1$, and $a_{2,1} \equiv \gamma_2$.

CEA formulas	Sample property measured	Heat capacity per
$a_k = (a_{1,k} - a_{2,k})\eta_m + a_{2,k} \quad \forall k$		
$\gamma_r = -\gamma_2\eta_m + \gamma_2$	mass	mass
$C_{\text{es}} = \eta_m^{-1}\Delta C_p + \gamma_1 T$		
$a_k = (a_{1,k} - a_{2,k})\eta_V + a_{2,k} \quad \forall k$		
$\gamma_r = -\gamma_2\eta_V + \gamma_2$	volume	volume
$C_{\text{es}} = \eta_V^{-1}\Delta C_p + \gamma_1 T$		
$a_k = (a_{1,k} - a_{2,k})\eta_n + a_{2,k} \quad \forall k$		
$\gamma_r = -\gamma_2\eta_n + \gamma_2$	a.o.s. ^a	a.o.s.
$C_{\text{es}} = \eta_n^{-1}\Delta C_p + \gamma_1 T$		
$a_k = (a_{1,k} - \nu a_{2,k})\eta_m + \nu a_{2,k} \quad \forall k$		
$\gamma_r = -\nu\gamma_2\eta_m + \nu\gamma_2$	mass	a.o.s.
$C_{\text{es}} = \eta_m^{-1}\Delta C_p + \gamma_1 T$		

^aThe a.o.s. of a two-component sample could be directly measured by a titration process, with two titrating reagents matched to the two components. However, this cumbersome process destroys the sample and would therefore have to be performed *after* the sample has been measured. It further requires detailed knowledge of the two components and is therefore unlikely to be used for our purpose. We nevertheless include the formulas for this situation for the sake of completeness.

Including $C_2^{\text{mag}} = \gamma_2^{\text{mag}} T$ extends the CEA as follows: Equations (9) and (13) from the

main text describing the γ - and the ΔC_p -slope-line are modified slightly to

$$\gamma = [\gamma_1 - (\gamma_2 + \gamma_2^{\text{mag}})]\eta_m + (\gamma_2 + \gamma_2^{\text{mag}}) \quad (\text{D1})$$

$$-d(\Delta C_p)/dT = (\gamma_1 - \gamma_2^{\text{mag}})\eta_m + \gamma_2^{\text{mag}}, \quad (\text{D2})$$

while Eq. (7) describing the γ_r -line remains the same:

$$\gamma_r = -\gamma_2\eta_m + \gamma_2. \quad (\text{D3})$$

In other words, the γ - and the ΔC_p -slope-line are changed in that their y -intercept is being moved up slightly by γ_2^{mag} .

A simultaneous fit of all three lines using γ_1 , γ_2 , γ_2^{mag} , and ΔU_1 as fit parameters, results in parameters identical within experimental error to the results from the analysis without a C_2^{mag} term: γ_1 increases by 0.6 % to $79.6 \mu\text{J/g/K}^2$ and ΔU_1 increases by 0.3 % to $863 \mu\text{J/g}$. γ_2^{mag} turns out to be $4.9 \mu\text{J/g/K}^2$, i.e. about 6 % of the normal state Sommerfeld coefficient γ_1 . The refined fit is shown in Fig. 9.

The superconducting electronic heat capacity $C_{\text{es}}(T)$ on a global scale is well represented by the extracted γ_1 using Eq. 12 (cf. Fig. 5). Plotting $C_{\text{es}}(T)$ on a logarithmic scale, however, emphasizes the lowest temperatures and it is thus important to include the effects of the γ_2^{mag} term:

$$C_{\text{es}}(T) = \eta_m^{-1}\Delta C_p + [\gamma_1 + (\eta_m^{-1} - 1)\gamma_2^{\text{mag}}] T. \quad (\text{D4})$$

Based on this, we have chosen effective Sommerfeld coefficients for the calculation of $C_{\text{es}}(T)$ by optimizing the congruence among the curves (inset of Fig. 5). The so-obtained coefficients follow the general trend $\gamma_1 + (\eta_m^{-1} - 1)\gamma_2^{\text{mag}}$, showing that the inclusion of $\gamma_2^{\text{mag}}T$ is reasonable. It also becomes clear that magnetic impurities have a significant effect on the extraction of $C_{\text{es}}(T)$ at small superconducting volume fractions and low temperatures.

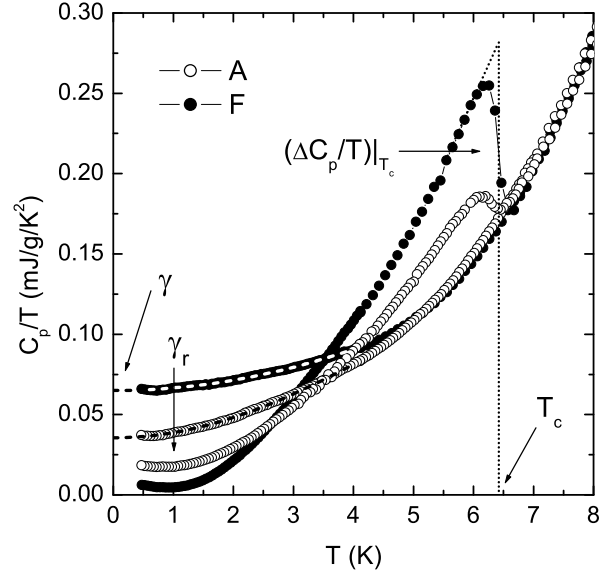


FIG. 1: Specific heat divided by temperature C_p/T for samples A and F at 0 T and 12 T. We extract the Sommerfeld coefficient γ by fitting the data from 1 K to 4 K to $C_p/T = \gamma + \beta T^2 + DT^4$ (shown by dashed lines). The residual coefficient γ_r is the C_p/T value at 1 K and 0 T, and T_c is chosen such as to balance the entropy. The residual Sommerfeld coefficient γ_r , the normal-state coefficient γ , and the specific heat jump at T_c , $\Delta C_p|_{T_c}/T_c$, vary among the various samples measured in a way that is a typical signature of a metallic second component. These observations form the basis for the condensation energy analysis (CEA) presented here.

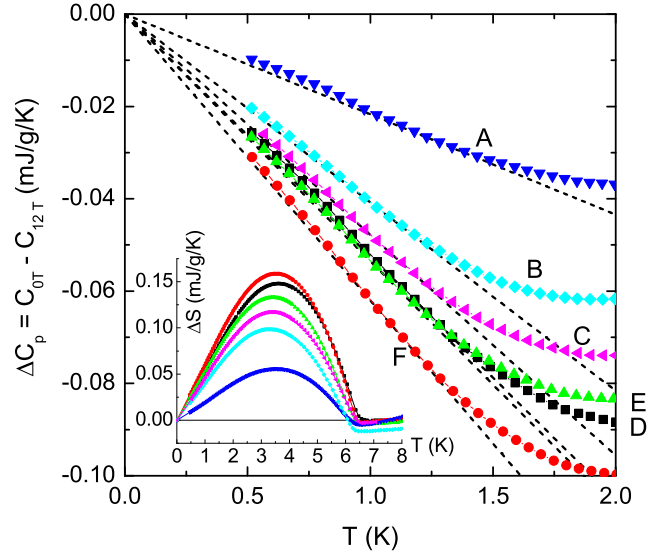


FIG. 2: (Color online) Low temperature heat capacity difference ΔC_p for the six samples measured in this study. At these temperatures $C_{es} \ll \gamma_1 T$ and therefore $\Delta C_p = -\gamma_1 \eta_m T$, i.e. ΔC_p is linear in T and the slope is proportional to η_m , varying from sample to sample. The inset shows the difference in entropy between the superconducting and normal state $\Delta S(T) = \int_T^{T_c} \Delta C_p(T')/T' dT'$.

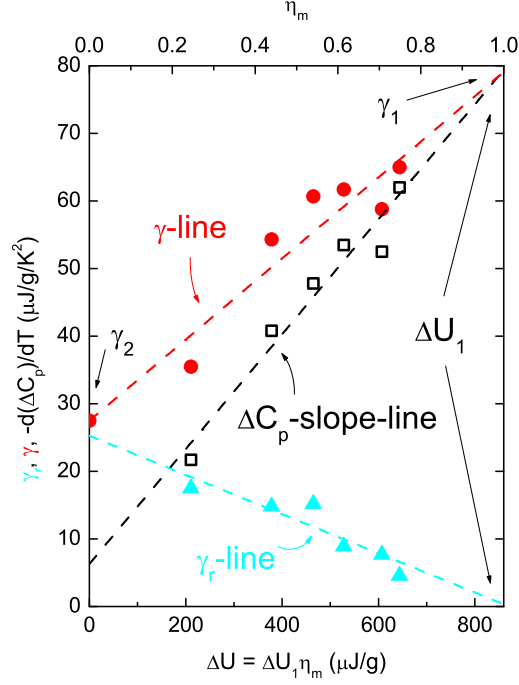


FIG. 3: (Color online) Summary of the data analysis for the six different RbOs_2O_6 samples and the OsO_2 sample at $\Delta U = 0$. Plotted vs the condensation energy are the measured Sommerfeld coefficient γ , the residual Sommerfeld coefficient γ_r , and the slope from ΔC_p vs T at low temperatures. All quantities are directly extracted from measurement (Figs. 1 and 2) and they all depend linearly on the superconducting mass fraction $\eta_m = \Delta U / \Delta U_1$, see Eqs. (7), (9), and (13). Thus a linear fit of these data is shown as γ -line, γ_r -line, and ΔC_p -slope-line respectively. The plot allows the extraction of γ_1 , γ_2 , and ΔU_1 at a glance and serves as a check for the consistency of the analysis.

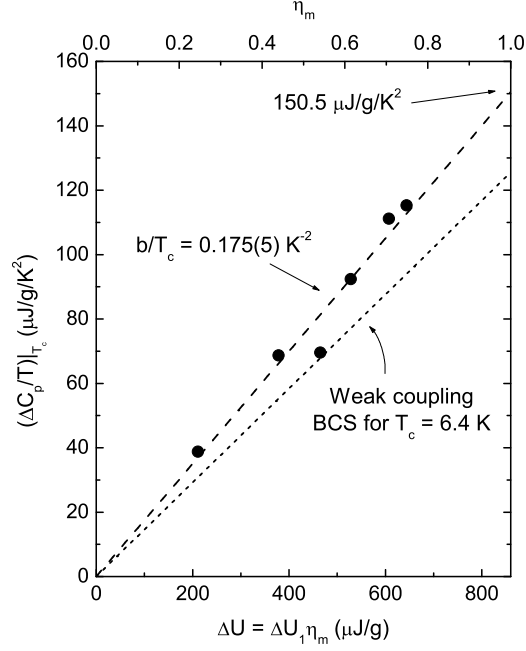


FIG. 4: The measured specific heat jump at T_c , $\Delta C_p|_{T_c}/T_c$, is proportional to the measured condensation energy. A linear fit using $\Delta C_p|_{T_c}/T_c = b/T_c \cdot \Delta U$ with b/T_c as a fit parameter gives $b/T_c = (0.175 \pm 0.005) \text{K}^{-2}$. For comparison, the BCS weak coupling $b/T_c = 0.146$ for $T_c = 6.4 \text{K}$ is also shown. The specific heat jump for RbOs_2O_6 is $150.5 \mu\text{J/g/K}^2$, resulting in $\Delta C_p|_{T_c}/(\gamma_1 T_c) = 1.9$, and thus a coupling parameter $\lambda_{\text{ep}} \approx 1$.

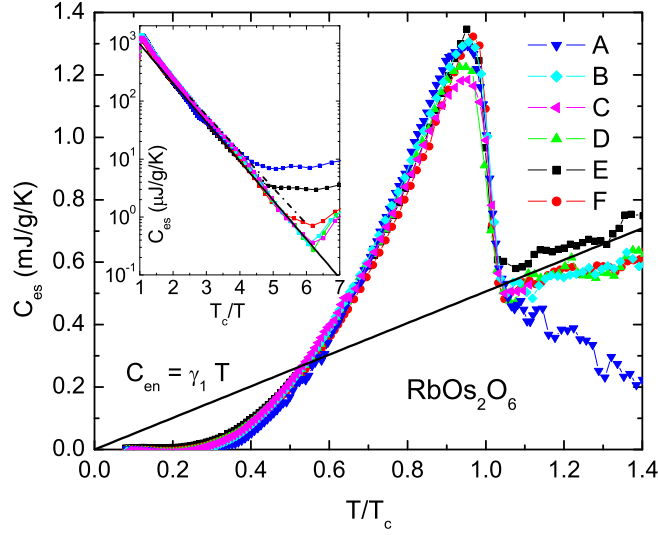


FIG. 5: (Color online) Superconducting electronic specific heat $C_{\text{es}}(T) = \eta_m^{-1} \Delta C_p + \gamma_1 T$ for all measured samples showing a universal behavior when scaled appropriately. The inset shows the superconducting electronic specific heat of RbOs_2O_6 showing close quantitative agreement with conventional superconducting behavior. The solid line is a best fit to the data and indicates the expected behavior from an isotropic gap: $C_{\text{es}} = 9 \gamma_1 T_c \exp(-1.55 T_c/T)$. For comparison the dash-dotted line shows the expected behavior from weak coupling BCS. The deviations at very low temperatures are due to scattering from various minute impurities.

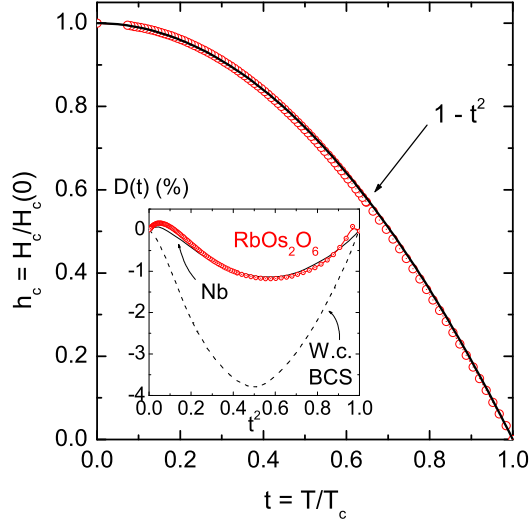


FIG. 6: (Color online) The reduced critical field $h_c(t) := H_c(T)/H_c(0\text{ K}) = \sqrt{\Delta U_1(T)/\Delta U_1(0\text{ K})}$ of sample F. The inset shows the deviation $D(t) := h_c(t) - (1 - t^2)$ from a simple $1 - t^2$ behavior for a weak coupling BCS superconductor, niobium, and RbOs_2O_6 . The deviation function of RbOs_2O_6 closely matches the data for Nb from Ref. [17]. The critical field at 0 K is $H_c(0\text{ K}) = 1249\text{ Oe}$.

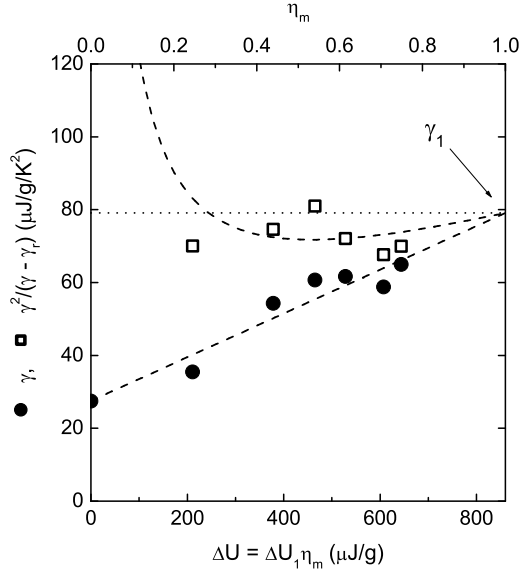


FIG. 7: Two different approaches to estimate the Sommerfeld coefficient of RbOs_2O_6 : The estimate $\gamma^2/(\gamma - \gamma_r)$ compared to the coefficient γ . Down to a superconducting mass fraction of $\eta_m \approx 20\%$, $\gamma^2/(\gamma - \gamma_r)$ is the better approximation to the true Sommerfeld coefficient γ_1 than γ .

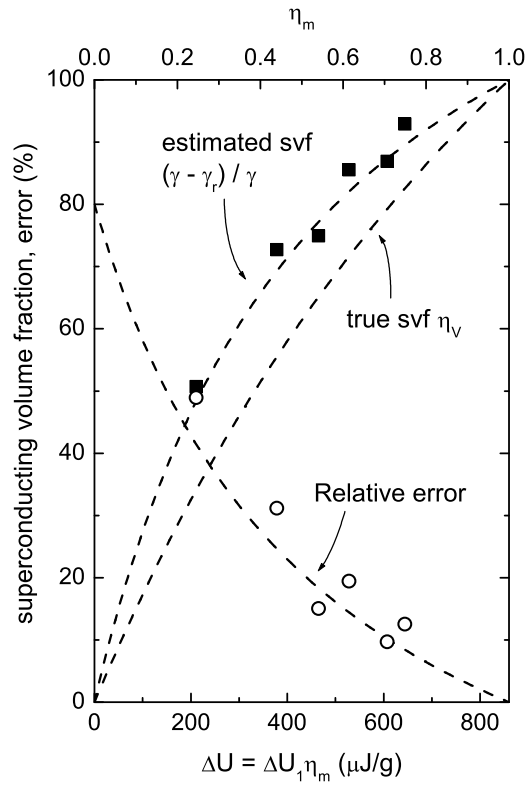


FIG. 8: The estimated superconducting volume fraction (svf) $(\gamma - \gamma_r)/\gamma$ compared to the true superconducting volume fraction η_V plotted as a function of the condensation energy ΔU . With OsO_2 as the second component, we calculated the ratio of the mass densities $\mu \approx 0.63$ and use it to evaluate η_V . The Figure also shows the relative error which reaches a maximum of 80% at $\eta_m = 0$.

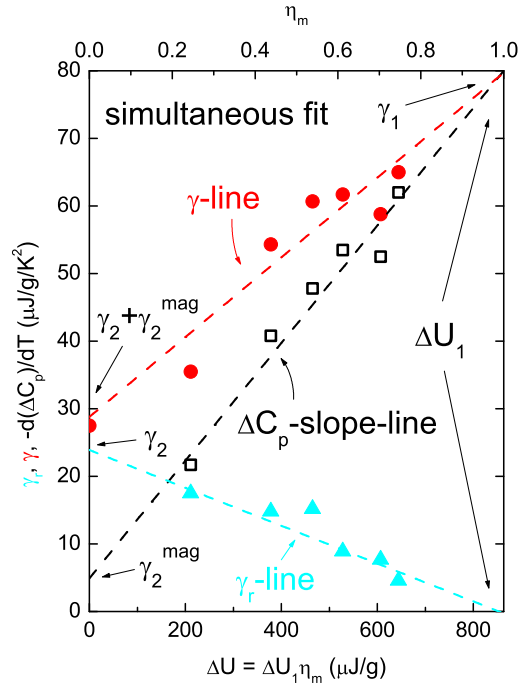


FIG. 9: (Color online) Refined CEA including a C_{mag} term: The data are simultaneously fitted to the γ -, ΔC_p -slope-, and the γ_r -line, see Eqs. (D1) to (D3). The result is essentially the same as when the lines are fitted separately (cf. Fig. 3).